INSTITUTE OF PHYSICS PUBLISHING NANOTECHNOLOGY
Nanotechnology **17** (2006) 1046–1051 doi:10.1088/0957-4484/17/4/034

Deterministic shape-selective synthesis of nanowires, nanoribbons and nanosaws by steady-state vapour-transport

A Colli[1], A Fasoli[1], S Hofmann[1], C Ducati[2], J Robertson[1] and A C Ferrari[1]

[1] Department of Engineering, University of Cambridge, Cambridge CB3 0FA, UK
[2] Department of Materials Science and Metallurgy, University of Cambridge, Cambridge CB2 3QZ, UK

E-mail: ac458@cam.ac.uk (A Colli)

Received 19 September 2005
Published 30 January 2006
Online at stacks.iop.org/Nano/17/1046

Abstract
We demonstrate the deterministic shape-selective synthesis and growth of CdSe nanowires, nanosaws and nanoribbons by a simple vapour-transport process in a tube furnace. The key step, in order to achieve reproducible shape selectivity for a given set of deposition parameters, is to exclude any effects of the temperature ramping. We prove that an efficient precursor-flow shutter is achieved just by varying the total furnace pressure. We then present a shape-diagram linking the different nanocrystals morphologies to only two parameters: powder and substrate temperature. These are varied in the 550–700 °C and 400–600 °C range, respectively. A model explaining the shape control is discussed.

1. Introduction

High-aspect-ratio semiconductor nanostructures are of great interest due to their potential applications in electronics and photonics [1–4]. They can be grown in a variety of different shapes [5–10] such as nanowires (NWs), nanoribbons (NRs) and nanosaws (NSs). As post-growth manipulation of nanostructures is difficult and expensive, their full potential will only be realized when they can be directly grown into devices. Hence, there is the need for general approaches to achieve shape-selectivity and position-selectivity. Shape-selectivity is the deterministic control of the nano-structure morphology. Position-selectivity is the deterministic growth into specific device locations.

So far, wet-chemistry is the most successful technique for shape-selective synthesis of quantum dots, wires, tetrapods and multi-branched heterostructures [9, 11]. A great advantage of this approach is that it does not require an expensive experimental set-up. However, the nanocrystals length typically does not exceed a few hundreds nanometres, which limits their suitability for some applications [12]. Also, they cannot be selectively grown in defined positions on a substrate, but require post-deposition handling. In contrast, molecular-beam epitaxy (MBE) [10, 13], chemical-beam epitaxy (CBE) [14, 15] or metal-organic chemical vapour deposition (MOCVD) [16, 17] allow patterned growth of NWs with lengths up to tens of micrometres, together with a high level of control over the deposition parameters. However, these are expensive experimental set-ups. In the case of CBE or MOCVD, the use of organic precursor gases can result in a systematic single-type background doping due to residual carbon, as shown by the n-type behaviour of as-deposited nanowires [15].

Vapour transport is a widely available technique. In principle, it combines the advantages of both wet-chemistry and molecular beam techniques. A single-zone quartz tube furnace is one of the simplest and most popular methods to implement vapour transport [6–8, 18]. It has been extensively used in the literature by a number of different groups to deposit a variety of different shapes of semiconductor nanocrystals [7, 8, 18–20]. However, a close inspection of the published literature shows that, for a given material, the growth of a certain nanocrystal shape is not uniquely linked to a fixed set of deposition conditions. As an example, Wang *et al* [21, 22] reported for the same nominal deposition conditions the growth of nanobelts in [21] and of nanocombs

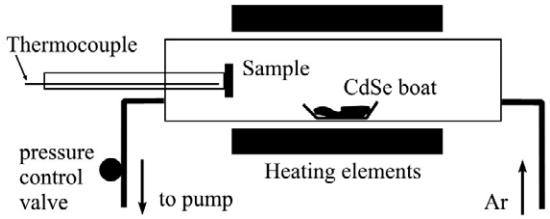

Figure 1. Schematic diagram of the experimental setup.

in [22]. Furthermore, there are reports where the desired nanocrystal shape is just a fraction of the total nanostructure yield, i.e. *different shapes are present on the same sample* (see, e.g. [8]). These contradictory results can be easily understood if one considers that in a quartz tube furnace there are normally no shutters providing sharp growth interruptions (unlike, e.g., MBE). Thus, the *nominal* deposition parameters *are not fully representative*, since evaporation and deposition also occur during the temperature ramps and not just when the nominal steady state conditions are reached [21]. This crucial aspect in vapour-transport growth has been so far overlooked in the literature. Thus, even if various groups have developed their own peculiar procedures to achieve certain nano-crystal shapes, these procedures are not generally applicable and do not allow the fully deterministic and reproducible growth of crystal shapes selected *a priori*.

In this paper, we propose a simple and generally applicable method to achieve fully deterministic and reproducible growth of nanowires, nanosaws and nanoribbons by vapour transport. We show that an efficient precursor-flow shutter can be implemented just by varying the total furnace pressure. This avoids any deposition on the substrate during the temperature ramps and allows us to start (and stop) the synthesis only when steady state conditions are reached. This is a key step in order to achieve reproducible shape selectivity. We then present a shape-diagram linking the different nano-crystals morphologies to only two parameters: powder and substrate temperature. We show that, once any transient behaviour is avoided, the transition between the different nanocrystals shapes is ruled by a similar growth kinetic to that controlling the shape transitions in semiconductor epitaxy. Once the shape is decided, we can combine shape-selectivity with position-selective growth by patterning a metal seed on the substrate [5, 16, 17]. We select CdSe as a test system, since it is one of the most studied II–VI materials in nanotechnology [8, 9, 11].

2. Experimental details

We use the single-zone furnace reactor shown schematically in figure 1. The quartz tube is 60 cm long and has a cross-sectional area of 20 cm^2. First, a thin (0.5–1.5 nm) Au film is thermally evaporated onto an oxidized Si surface and patterned using ultraviolet or e-beam lithography [23]. The substrate is then mounted vertically on the sealed tip of an inner quartz feed-through (1 cm diameter). This allows an accurate substrate positioning in the furnace tube and real-time monitoring of the growth temperature with a thermocouple directly in contact with the substrate via the quartz feed-through, figure 1. Since the furnace is single zone, the powder

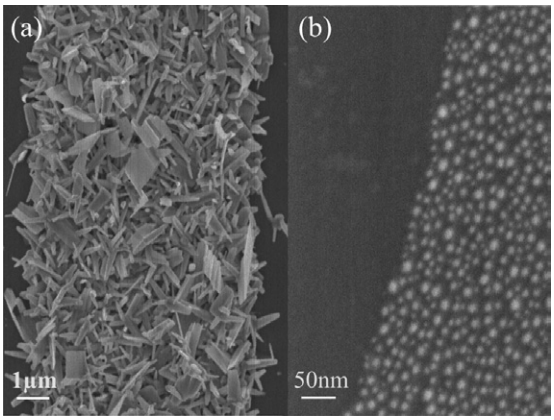

Figure 2. FE-SEM images of the substrate after a heating ramp to 700 °C. The Ar pressure is (a) 100 mbar; (b) 1 bar. No CdSe nucleation is found on (b), the dots are the uncoated Au catalyst islands.

temperature (T_P) is directly set by the furnace temperature control. The substrate temperature (T_S) is defined by its relative position with respect to the centre of the furnace, according to the empirical relation:

$$T_S = T_P - G_T(d_S - d_0) \quad (1)$$

where d_S is the sample distance from the centre of the furnace, d_0 is the distance where the temperature gradient begins, and G_T is the temperature gradient along the tube axis. For our set-up, $d_0 \sim 16.5$ cm and $G_T \sim 35\,°C\,cm^{-1}$. A quartz boat filled with commercial CdSe powder (Alpha Aesar, 99.995%) is placed in the centre of the main tube, which is evacuated to a base pressure of $\sim 10^{-3}$ mbar. The furnace is then heated at a rate of 10 °C min^{-1} to a target temperature chosen in the 500–700 °C range, while the pressure is kept at 1 bar in a constant 100 sccm Ar flow. When both the precursor powder and the Au-coated Si substrate reach the final target temperatures, the pressure is quickly reduced to 100 mbar, and maintained at this value for a deposition time of 1 h. Then, the furnace is left to cool down to room temperature while the pressure is raised again to 1 bar in a constant 100 sccm Ar flow. The structure of the resulting CdSe nanocrystals is investigated by field-emission scanning electron microscopy (FE-SEM) coupled with energy dispersive x-ray spectroscopy (EDX) and high-resolution transmission electron microscopy (HRTEM, 400 kV).

3. Results and discussion

3.1. Precursor-flow shutter

We first demonstrate how to implement an efficient precursor-flow shutter just by varying the furnace pressure. Figure 2(a) shows CdSe nanostructures nucleated on an Au pattern during a heating ramp to $T_P = 700\,°C$, $T_S = 600\,°C$, at a constant Ar pressure of 100 mbar for the whole process. The substrate is immediately cooled at the end of the heating ramp, resulting in a negligible steady-state growth time. However, from figure 2(a) it is evident that significant growth occurs during the ramping. As a consequence, nanostructures in figure 2(a)

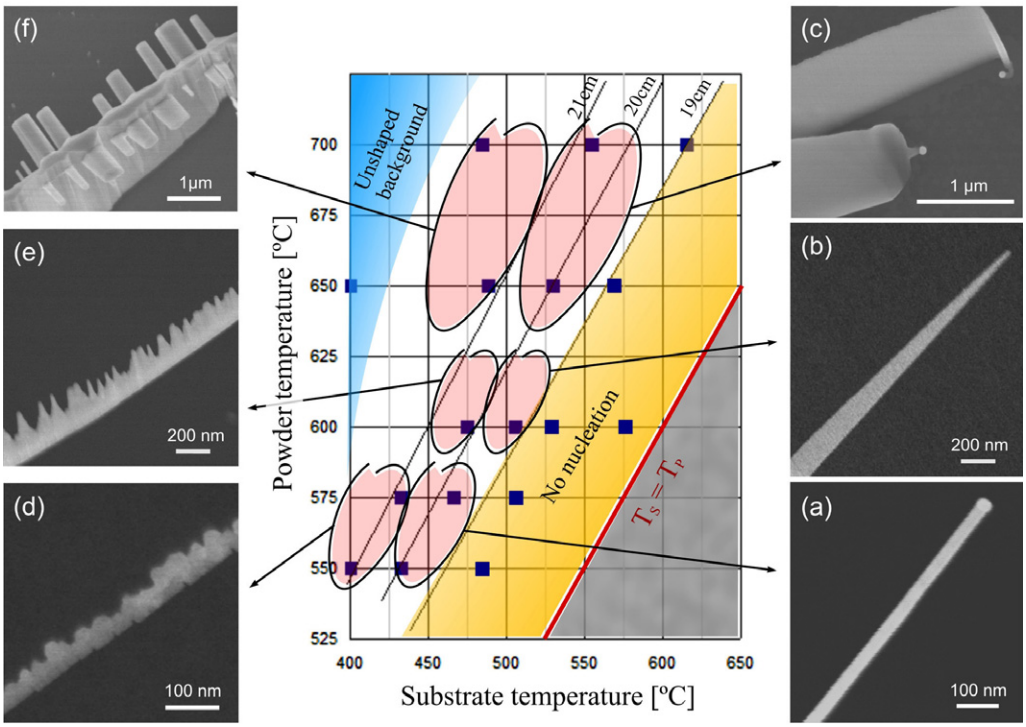

Figure 3. Shape-diagram for CdSe nanocrystal morphology control. The solid lines represent the T_P versus T_S relation for a given sample-boat distance. Squares indicate growth conditions directly tested. The thick line (red online) represents the $T_P = T_S$ limit. The unphysical $T_P < T_S$ region is represented by the shaded dark-gray triangle. In the shaded trapezoid region (orange online) no nucleation occurs. In the shaded top left triangular region an unshaped background is deposited. (a)–(f) Representative SEM pictures for samples grown in the marked regions. (a) nanowires, (b) tapered nanowires, (c) nanoribbons, (d) nanosaws (e) tapered nanosaws, (f) nanocantilevers/nanocombs.

(This figure is in colour only in the electronic version)

are not representative of the nominal T_P and T_S and their shape depends in a complex way on the heating ramp. On the other hand, figure 2(b) shows the Au-coated substrate after ramping to the same target T_S and T_P as in figure 2(a), but at a constant Ar pressure of 1 bar. In this case also, the substrate was immediately cooled at the end of the heating ramp. No nanostructures are seen in figure 2(b) and neither Cd nor Se is detected on the surface by EDX. The only effect of the heating process is to coarsen the initial patterned Au film to create a nano-island topography. Similar results are obtained for all the T_P–T_S we use for the experiments described below. This demonstrates that a simple change in the Ar pressure acts as an effective precursor-flow shutter avoiding any unwanted deposition.

The precursor-flow shutter can be explained in terms of a dominant diffusion regime. Vapour transport along a tube is partially due to the carrier gas flow and partially due to concentration and thermal diffusion effects [24]. If the tube is several cm in diameter, the velocity of the inert gas flow is very low, and diffusion can become dominant. For our system, when the inlet and outlet flows are stable to 100 sccm (irrespective of the total pressure), the flow velocity in the tube is only 5 cm min^{-1}, as derived from the ratio of volume flow to the tube cross section area (100 sccm/20 cm^2). If vapour transport were just due to gas carrier flow, condensation should only happen downstream. However, during growth at 100 mbar, significant condensation happens *both downstream and upstream*. This implies that the precursor flow impinging on the substrate is mainly driven by diffusive transport. We can then understand the effect of different total pressures on diffusive transport. The diffusion coefficient is inversely proportional to the total pressure [24]. Thus, increasing the pressure by an order of magnitude lowers the diffusion coefficient at least by a factor of 10. As a consequence, the CdSe precursor flow will be highly suppressed. We stress that, to a first approximation, this effect is entirely due to a different diffusion regime, since the saturation vapour pressure of CdSe is only a function of the powder temperature and is independent of the Ar partial pressure [24]. A complete description of the precursor flow process is non-trivial. Additional effects, such as non-saturation at the boat position or gas un-mixing along the temperature gradient, could also contribute in making the precursor-flow shutter more efficient [24].

3.2. Shape-diagram

We now consider the effect of T_S and T_P on the morphology of the nanostructures grown when steady state conditions are reached. The shape-diagram in figure 3 is the pivotal result of this paper. It summarizes the morphology dependence of the CdSe nanocrystals as a function of T_P and T_S. All the different morphologies previously reported in the literature for vapour-transport growth fall in the explored range of parameters. Note that in all cases growth is only observed on the catalyst pattern.

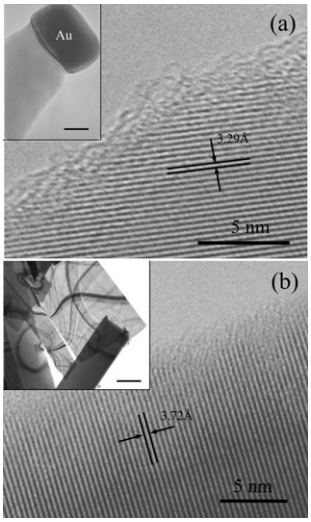

Figure 4. HRTEM images of (a) CdSe nanowire and (b) nanoribbons, grown in the same conditions as those in figures 2(a) and (c). Scale bars in the insets are (a) 200 nm; (b) 20 nm. The plane spacing indicated in (a) and (b) match the $(1\bar{1}1)$ and $(1\bar{1}0)$ planes of wurtzite CdSe, respectively.

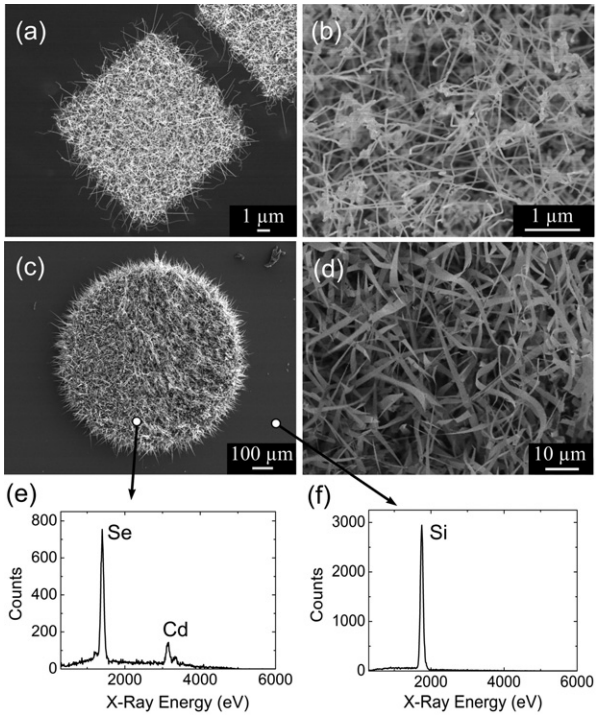

Figure 5. Patterned growth of ((a), (b)) nanowires and ((c), (d)) nanoribbons, on a Si substrate. ((b), (d)) Higher magnification images of (a), (c) showing the presence of a single nanocrystal shape. ((e), (f)) EDX spectra inside and outside the pattern in (c), showing neither Cd nor Se are deposited outside the region defined by the Au catalyst. Note that the EDX spectrum on the nanocrystals reveals a stoichiometric CdSe composition, once the intensities are normalized by the different cross-sections.

We first consider the case of low T_P (e.g. 550 °C). For $T_S > 470$ °C no nucleation occurs. $T_S = 430$–470 °C results in thin and uniform CdSe NWs, ∼50 nm in diameter, catalytically grown from Au particles (figures 3(a) and 4(a)). Finally, for $T_S < 430$ °C, we get CdSe nanosaws (figure 3(d)).

We then consider the case of high T_P. If this is relatively high (e.g. 650 °C), no nucleation occurs for $T_S > 550$ °C. CdSe nanoribbons are formed for $520\,°C < T_S < 550\,°C$ (figures 3(c) and 4(b)). For $T_S < 500$ °C, thicker structures of irregular shape are deposited (figure 3(f)), which could be described as nanocantilevers or nanocombs [22]. $T_S \sim 400$ °C gives unshaped polycrystalline agglomerates.

Figures 4(a) and (b) show HRTEM images of typical CdSe NWs and NRs, corresponding to the SEM images of figures 3(a) and (c). Both NWs and NRs are highly crystalline and virtually free of lattice defects. The nanowire in figure 4(a) shows a set of lattice fringes matching with the $(1\bar{1}1)$ planes of wurtzite CdSe having the $[10\bar{1}]$ axis parallel to the electron beam. Figure 4(b) shows a set of lattice fringes corresponding to the $(1\bar{1}0)$ planes of wurtzite CdSe close to the [111] axis. This implies a high-quality crystal growth when the deposition conditions are properly chosen in the shape-diagram of figure 3.

Thus, we can use figure 3 to select the growth conditions for the particular nanocrystal shape we are interested in. Patterns of the selected nanocrystals can then be directly grown on the oxidized Si substrate by using Au seeds as shown in figures 5(a)–(d). The metal seed acts as the preferred site for deposition of the vapour [5], due to the much higher sticking coefficient when compared to silicon oxide [25]. The EDX spectra in figure 5 demonstrate that neither Cd nor Se are deposited in these conditions outside the Au patterns. They also prove the 50:50 stoichiometry of the deposited CdSe nanocrystals. Similarly, we detect a photoluminescence signal only inside the patterns, while no appreciable intensity is measured outside. Only in the 'unshaped background' region of figure 3 can Cd and Se be detected on the oxidized Si surface, indicating a regime not appropriate for either shape-selectivity or positional-selectivity.

Here we stress again that the combination of shape selectivity and position selectivity *cannot be achieved without the use of the pressure-shutter*. Figure 2(a) is a clear example of this. If the substrate is allowed to lie horizontally in the furnace tube (this is typically the case in most of the previous reports, see, e.g. [19, 20, 26]) the effect is even more dramatic. Figures 6(a) and (b) show nanostructures grown on a ∼8 mm long substrate lying horizontally in the furnace tube without the use of the pressure shutter. Figure 6(a) shows a sample area close to the downstream substrate border, while figure 6(b) shows a region close to the upstream one. The deposition parameters were chosen to target the nanoribbon regime of figure 3. However, nanocrystals in figure 6(a) are totally different from those in figure 6(b). The presence of thin nanowires in figure 6(a) contrasts the prediction of the shape-diagram for the nominal T_P, T_S used in the experiment. On the other hand, figures 6(c) and (d) show the analogous positions on the substrate after a growth experiment in the same nominal T_P, T_S, *but with the use of the pressure shutter*. In this case, the morphology is homogeneous over the whole sample area.

Note that in figure 6 we adopted the horizontal substrate geometry to directly compare with previous literature reports. However, we wish to stress that, in general, the horizontal

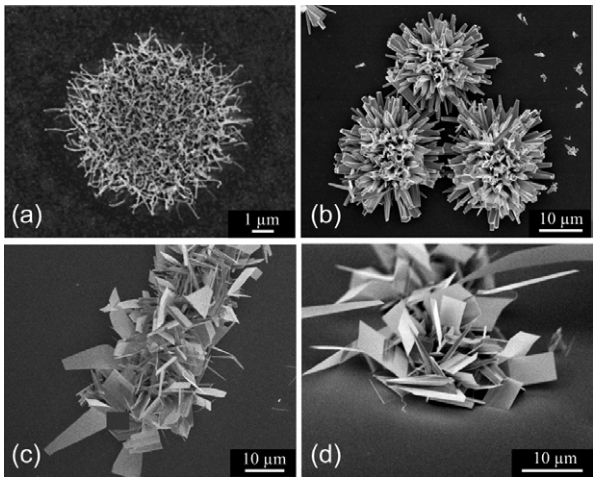

Figure 6. Comparison of CdSe nanostructures grown on patterned substrates lying horizontally in the furnace reactor, ((a), (b)) without and ((c), (d)) with the use of the pressure shutter. ((a), (c)) show the downstream edges of the samples, while ((b), (d)) show the upstream ones. T_P and T_S were chosen in the nanoribbon regime of figure 3.

substrate geometry should be avoided if one wants to get the maximum uniformity and shape selectivity. Indeed, the horizontal substrate geometry, even when using the pressure shutter, is prone to give an in-homogeneous morphology distribution along the sample surface since the local temperature changes along the substrate length, according to equation (1). For the 8 mm long sample in figure 6, the temperature difference between the upstream and downstream edge is ∼25–30 °C. This, according to figure 3, is small enough to keep T_S within the nanoribbon regime. However, it is clear that this effect can become a concern for larger substrates. Therefore, for the experiments reported in figure 3 we used the vertical substrate loading as the standard configuration. This ensures, together with an improved experimental control, a uniform and reproducible shape-selectivity close to 100%.

3.3. Growth mechanism

We now discuss the mechanism ruling the shape-diagram of figure 3. We propose that the change in nanocrystal shape is determined by processes very similar to those controlling film morphology in semiconductor epitaxy [27]. It is well known that the growth kinetics in semiconductor epitaxy is driven by the interplay of precursor impinging on the substrate and thermal desorption at the sample surface [27]. For fixed substrate temperature, higher precursor flows result in higher growth rates. For fixed precursor flow, lowering the substrate temperature enhances epitaxial growth. If this further drops below a certain threshold, epitaxial growth can switch from a layer-by-layer regime to three-dimensional nucleation [27]. This is triggered by a combination of reduced desorption and low surface mobility of the adsorbed atoms.

In our case, T_P controls the CdSe vapour pressure at the boat position [28]. Thus, for fixed Ar pressure, T_P also determines the amount of Cd and Se_2 arriving on the substrate. T_S defines the available thermal energy for desorption and surface diffusion. The starting point in the shape-diagram is the nucleation of a nanowire, figure 3(a). The catalyst sets the nucleation site and drives the one-dimensional growth [5, 6, 10, 14–17]. Nanoribbons grow epitaxially, layer by layer, from the side-walls of NWs [6], as shown by the shape-change from figure 3(a) to (c). This is confirmed by the presence of the Au catalyst at the end of the NR in figure 3(c). Such transition is achieved by increasing T_P, i.e. enhancing the epitaxial growth rate, combined with a proportional increase of T_S, which provides more thermal energy to maintain the layer-by-layer regime [27].

We can also explain the shape changes from figures 3(a) to (d) and from figures 3(c) to (f). Along the whole range explored, saws or appendices to the main structure are formed by lower T_S for a fixed T_P. This is a regime where the substrate thermal energy is not sufficient to promote a layer-by-layer epitaxial growth, due to the lower mobility of the adsorbed atoms. Thus, three-dimensional nucleation occurs [27]. The branched structures in figure 3(f) are then explained in terms of low-temperature 3D epitaxy on the flat NRs in figure 3(c). In particular, for the wurtzite crystal structure, branches of rectangular shape are expected [22]. Indeed, figure 3(d) represents for figure 3(a) a similar transition as that from figures 3(c) to (f). Note that the catalyst is also present at the end of the NSs, even if not shown in the NS sections of figures 3(d) and (f).

Our model is validated by the experiments represented in figures 3(b) and (e). The structures in figures 3(b) and (e) are grown in intermediate conditions between NW, figure 3(a), and NR, figure 3(c), and between NS, figure 3(d), and nanocombs, figure 3(f). Quite remarkably they show an intermediate shape. The structures are tapered but the epitaxial overgrowth is not complete, as expected.

We expect the shape-diagram of figure 3 to be quite general and to hold for a wide range of semiconductor nanomaterials. Indeed, we have previously observed widening and tapering of ZnSe NWs in MBE growth when decreasing T_S for fixed precursor flow [10]. Also, for small-diameter ZnSe NSs similar to those in figure 3(d), the teeth-like profile is often coupled with the formation of defects, such as crystal twinnings [10]. Figure 3 also explains the data of Jiang *et al* [18], who reported an increase in width of ZnS NRs for increasing T_P.

Different trends to those in figure 3 are sometimes found in the literature. For instance references [19, 20, 26], reported the need to increase T_S (for fixed T_P) in order to promote epitaxial growth and have a morphology transition from NWs to NRs and nanosheets. In these papers, a variety of different morphologies are found in the same growth run, for fixed T_P, on substrates lying horizontally in the tube experiencing a T_S gradient. This is similar to that shown in figures 6(a) and (b) when no pressure-shutter is implemented. The shape-diagram in figure 3 shows that if we are in the NW growth regime, increasing just T_S leads to the no-nucleation zone, not to the NR region. A concomitant, significant increase in the CdSe precursor flow is needed to obtain NR formation. On the other hand, if we are in the NR regime, decreasing just T_S leads to the unshaped background region, not to the NWs region. We therefore conclude that in references [19, 20, 26], most likely due to the lack of precursor-flow shutter, the vapour density did vary along the furnace tube

for fixed nominal T_P, making systematic shape selectivity a challenge.

4. Conclusions

In summary, we demonstrated the deterministic and fully reproducible shape-selective growth of several morphologies of CdSe nanocrystals in a tube furnace vapour-transport deposition system. We showed how to implement a simple precursor-flow shutter by changing the total pressure in the furnace reactor to allow steady state nanostructure growth. This can be easily done for any vapour transport growth process in a quartz-tube and requires no mechanical parts. This is *essential* in order to ensure that the critical parameters T_S and T_P are fully representative of the observed nanostructure morphology. Indeed, we successfully applied the precursor-flow shutter for vapour-transport growth of Si nanowires. Also in this case no Si deposition is detected at high pressure. At low pressure Si nanowires are deposited both downstream and upstream. Once thermal gradients are eliminated, our results show that the transition from one nanocrystal shape to another is controlled just by the interplay of precursor impinging on the substrate and sample surface kinetics. These two general processes are ruled by the powder and substrate temperatures, respectively, and are the same mechanisms controlling the growth kinetics in semiconductor epitaxy.

Acknowledgments

The authors acknowledge funding from EU project CANAPE. ACF acknowledges funding from The Royal Society. SH acknowledges funding from Peterhouse, Cambridge.

References

[1] Hiruma K, Yazawa M, Katsuyama T, Ogawa K, Haraguchi K, Koguchi M and Kakibayashi H 1995 *J. Appl. Phys.* **77** 447
[2] Law M, Goldberger J and Yang P 2004 *Annu. Rev. Mater. Res.* **34** 83
[3] Duan X F, Huang Y, Agarwal R and Lieber C M 2003 *Nature* **421** 241
[4] Barrelet C J, Greytak A B and Lieber C M 2004 *Nano Lett.* **4** 1981
[5] Wagner R S and Ellis W C 1964 *Appl. Phys. Lett.* **4** 89
[6] Wagner R S, Ellis W C, Jackson K A and Arnold S M 1964 *J. Appl. Phys.* **35** 2993
[7] Wang Z L 2004 *Mater. Today* **7** 26
[8] Ma C, Ding Y, Moore D, Wang X D and Wang Z L 2004 *J. Am. Chem. Soc.* **126** 708
[9] Milliron D J, Hughes S M, Cui Y, Manna L, Li J B, Wang L W and Alivisatos A P 2004 *Nature* **430** 190
[10] Colli A, Hofmann S, Ferrari A C, Ducati C, Martelli F, Rubini S, Cabrini S, Franciosi A and Robertson J 2005 *Appl. Phys. Lett.* **86** 153103
[11] Huynh W U, Dittmer J J and Alivisatos A P 2002 *Science* **295** 2425
[12] Law M, Greene L E, Johnson J C, Saykally R and Yang P 2005 *Nat. Mater.* **4** 455
[13] Schubert L, Werner P, Zakharov N D, Gerth G, Kolb F M, Long L, Gosele U and Tan T Y 2004 *Appl. Phys. Lett.* **84** 4968
[14] Bjork M T, Ohlsson B J, Sass T, Persson A I, Thelander C, Magnusson M H, Deppert K, Wallenberg L R and Samuelson L 2002 *Appl. Phys. Lett.* **80** 1058
[15] Ohlsson B J, Bjork M T, Persson A I, Thelander C, Wallenberg L R, Magnusson M H, Deppert K and Samuelson L 2002 *Physica* E **13** 1126
[16] Hiruma K, Yazawa M, Haraguchi K, Ogawa K, Katsuyama T, Koguchi M and Kakibayashi H J 1993 *J. Appl. Phys.* **74** 3162
[17] Mårtensson T, Carlberg P, Borgstrom M, Montelius L, Seifert W and Samuelson L 2004 *Nano Lett.* **4** 699
[18] Jiang Y, Meng X M, Liu J, Xie Z Y, Lee C S and Lee S T 2003 *Adv. Mater.* **15** 323
[19] Fang X S, Ye C H, Zhang L D, Wang Y H and Wu Y C 2005 *Adv. Funct. Mater.* **15** 63
[20] Venugopal R, Lin P I, Liu C C and Chen Y T 2005 *J. Am. Chem. Soc.* **127** 11262
[21] Hughes W L and Wang Z L 2005 *Appl. Phys. Lett.* **86** 043106
[22] Wang Z L, Kong X Y and Zuo J M 2003 *Phys. Rev. Lett.* **91** 185502
[23] Hofmann S, Ducati C, Neill R J, Piscanec S, Ferrari A C, Geng J, Dunin-Borkowski R E and Robertson J 2005 *J. Appl. Phys.* **94** 6005
[24] Merten U and Bell W E 1967 *The Characterization of High-Temperature Vapors* (New York: Margrave) chapter 4
[25] Masson D P, Landheer D, Quance T and Hulse J E 1998 *J. Appl. Phys.* **84** 4911
[26] Dai Z R, Pan Z W and Wang Z L 2003 *Adv. Funct. Mater.* **13** 9
[27] Herman M A and Sitter H 1989 *Molecular Beam Epitaxy* (Berlin: Springer)
[28] Wosten W J 1961 *J. Phys. Chem.* **65** 1949